Neural crest survival and differentiation in zebrafish depends on *mont blanc/tfap2a* gene function

Alejandro Barrallo-Gimeno[1,*], Jochen Holzschuh[2,†], Wolfgang Driever[2] and Ela W. Knapik[1,‡,§]

[1]GSF, Institute for Mammalian Genetics, Ingolstaedter Landstrasse 1, D-85764 Neuherberg, Germany
[2]Developmental Biology, Institute Biology 1, University of Freiburg, Hauptstrasse 1, D-79104 Freiburg, Germany
*Present address: Institute of Neurobiology, "Ramón y Cajal" CSIC. Avenida Dr Arce 37, Madrid 28002, Spain
†Present address: Department of Developmental and Cell Biology, University of California Irvine, 5205 BioSci II, Irvine CA 92697-2300, USA
‡Present address: Developmental Biology, Institute Biology 1, University of Freiburg, Hauptstrasse 1, D-79104 Freiburg, Germany
§Author for correspondence (e-mail: ela.knapik@biologie.uni-freiburg.de)

Accepted 12 December 2003

Development 131, 1463-1477
Published by The Company of Biologists 2004
doi:10.1242/dev.01033

Summary

Neural crest progenitor cells are the main contributors to craniofacial cartilage and connective tissue of the vertebrate head. These progenitor cells also give rise to the pigment, neuronal and glial cell lineages. To study the molecular basis of neural crest differentiation, we have cloned the gene disrupted in the *mont blanc* (*mob^{m610}*) mutation, which affects all neural crest derivatives. Using a positional candidate cloning approach we identified an A to G transition within the 3′ splice site of the sixth intron of the *tfap2a* gene that abolishes the last exon encoding the crucial protein dimerization and DNA-binding domains. Neural crest induction and specification are not hindered in *mob^{m610}* mutant embryos, as revealed by normal expression of early neural crest specific genes such as *snail2*, *foxd3* and *sox10*. In addition, the initial stages of cranial neural crest migration appear undisturbed, while at a later phase the craniofacial primordia in pharyngeal arches two to seven fail to express their typical set of genes (*sox9a*, *wnt5a*, *dlx2*, *hoxa2/b2*). In *mob^{m610}* mutant embryos, the cell number of neuronal and glial derivatives of neural crest is greatly reduced, suggesting that *tfap2a* is required for their normal development. By tracing the fate of neural crest progenitors in live *mont blanc* (*mob^{m610}*) embryos, we found that at 24 hpf neural crest cells migrate normally in the first pharyngeal arch while the preotic and postotic neural crest cells begin migration but fail to descend to the pharyngeal region of the head. TUNEL assay and Acridine Orange staining revealed that in the absence of *tfap2a* a subset of neural crest cells are unable to undergo terminal differentiation and die by apoptosis. Furthermore, surviving neural crest cells in *tfap2a/mob^{m610}* mutant embryos proliferate normally and later differentiate to individual derivatives. Our results indicate that *tfap2a* is essential to turn on the normal developmental program in arches 2-7 and in trunk neural crest. Thus, *tfap2a* does not appear to be involved in early specification and cell proliferation of neural crest, but it is a key regulator of an early differentiation phase and is required for cell survival in neural crest derived cell lineages.

Key words: Neural crest, Apoptosis, Zebrafish, *tfap2a*, *mont blanc*, Craniofacial development, Pigment, Cranial ganglia, Muscle development

Introduction

The modern head is a major evolutionary accomplishment that allowed vertebrates to develop a predatory lifestyle (Gans and Northcutt, 1983; Manzanares and Nieto, 2003). Its main features are strong jaws suspended by the mandibular joints to the brain-protecting skull and a set of sensory organs (eye, ear, nose) for navigation. The head skeleton and face are mainly built of neural crest cells with contributions from ectoderm, endoderm and paraxial mesoderm (Le Douarin, 1982). In higher vertebrates, the neural crest cell progenitors arise from the dorsal edge of the neural folds at the time of neural tube closure; undergo a morphological transition from neuroepithelial to mesenchymal cells; and begin migration to remote parts of the body where they differentiate into craniofacial cartilage, cranial sensory neurons and glia, enteric neurons, pigment cells and other cell types. In zebrafish, where the central nervous system develops by a process of secondary neurulation, neural folds do not form and neural crest cells are specified from ectoderm at dorsal and dorsolateral aspects of the neural keel (Schilling and Kimmel, 1994).

Wnt, Bmp2/4 and TGFβ 1, 2 and 3 signaling pathways regulate the induction of multipotent neural crest progenitor cells and the newly specified premigratory neural crest progenitors express a unique set of transcription factors that includes Foxd3, Slug, Id2, Sox10 and Tcfap2a (Knecht and Bronner-Fraser, 2002). Subsequently, the neural crest cells turn off early markers like Foxd3, upregulate a new set of genes (e.g. cadherins 7 and 11, Rho proteins) and begin migration (Nieto, 2001). At this stage of development, neural crest cells originating in the midbrain migrate as a wave in a caudal direction. The first to migrate are the cells populating the pharyngeal arches and neuronal progenitors of the peripheral nervous system in the trunk. This first group of cells is followed by a second wave of migration supplying

cells to cranial ganglia in the head and pigment cells in the trunk (Kelsh and Raible, 2002). During migration, cells continue to proliferate and begin to express genes defining the cell lineage they are destined to form. The craniofacial neural crest expresses genes associated with formation and differentiation of mesenchymal condensations (e.g. *sox9a*, *wnt5a*, *dlx2*, *dlx6*, *dlx8*) (Chiang et al., 2001; Blader et. al., 1996; Richman and Lee, 2003), while the pigment cell lineages are marked by *mitfa*, *fms*, *kit* and *dct* (Kelsh and Raible, 2002; Rawls et al., 2001; Parichy et al., 2000; Goding, 2000). The neural crest cells are guided to their final destinations, change morphology and differentiate to mature derivatives. These processes have been well described by embryologists, but genetic and molecular data on genes and their function in neural crest induction, specification and differentiation has only recently begun to emerge. However, the genetic circuits that coordinate such complex developmental processes still remain unclear.

To gain further insight in the genetic control of neural crest differentiation, we have characterized the phenotype of zebrafish *mont blanc* (*mob*^{m610}) mutant embryos. Our results show that in *mont blanc* (*mob*^{m610}) mutant embryos, neural crest induction, specification and the initial stages of cranial neural crest migration appear undisturbed, while later in development, the craniofacial primordia in pharyngeal arches two to seven fail to form and trunk neural crest derivatives are severely reduced. Further analysis revealed that the *mob*^{m610} mutant neural crest cells, with the exception of those in the first pharyngeal arch, are unable to undergo proper differentiation, abort migration and die by apoptosis. Using linkage analysis and genetic mapping, we have identified the transcription factor *ap-2 alpha* (*tfap2a*) as the gene altered by the *mob*^{m610} mutation. Consistent with a role during neural crest cell migration, we found that *tfap2a* is expressed in early neural crest progenitors and in migratory neural crest cells. Our findings indicate that *tfap2a/mob* is essential for neural crest cell differentiation and survival and that it is specifically required for normal development of arches 2-7 and trunk neural crest.

Materials and methods

Fish maintenance and breeding

Fish were raised and kept under standard laboratory conditions at 28.5°C (Westerfield, 1995). Embryos were staged and fixed at specific hours or days post fertilization (hpf or dpf) as described by Kimmel et al. (Kimmel et al., 1995). To better visualize internal structures, in some experiments embryos were incubated with 0.2 mM 1-phenyl-2-thiourea (Sigma) to inhibit pigment formation. *mob*^{m780} and *mob*^{m610} were previously described as two *mont blanc* alleles by Neuhauss et al. (Neuhauss et al., 1996). We have sequenced *mob*^{m780} and *mob*^{m610} and found that the lesion was in the same base pair of the gene. We have scrutinized the original pedigrees and found that the two founder fish were derived from one mutagenized male, suggesting that the two alleles are in fact subsequent isolations of the same mutational event. Therefore, we will refer to the mutation hereafter as *mob*^{m610}. The *mob*^{m610} allele was kept in AB strain background for phenotype analysis and crossed into Tuebingen-long fin (TL) background for genetic mapping experiments (Knapik et al., 1996). We have also analyzed the neural crest phenotype in the *mob*^{m819} allele that was independently isolated in an ENU-mutagenesis screen for noradrenergic phenotypes [described in detail by Holzschuh et al. (Holzschuh et al., 2003)].

Cartilage staining

The Alcian Blue staining protocol was modified from Neuhauss et al. (Neuhauss et al., 1996). Embryos at 3 to 5 dpf were anesthetized in 0.02% buffered tricaine (Sigma) and fixed overnight in 4% phosphate-buffered paraformaldehyde (PFA) at 4°C. After washing in phosphate-buffered saline (PBS), embryos were bleached in 1 ml 10% hydrogen peroxide (H_2O_2) supplemented with 50 μl of 2 M KOH for 1 hour. They were then stained overnight in 0.1% Alcian Blue dissolved in acidic ethanol (70% ethanol, 5% concentrated hydrochloric acid), washed extensively in acidic ethanol, dehydrated and stored in 80% glycerol. For better exposure of cartilage elements embryos were digested with proteinase K.

Genetic mapping and cloning

mob^{m610} was mapped in a F2 intercross using bulked segregant analysis (Michelmore et al., 1991). *mob*^{m610} heterozygous fish and wild-type TL fish were crossed to obtain the F1 generation. In sibling crosses we identified mutation-carrying F1 heterozygotes and F2 embryos were scored for the *mob*^{m610} phenotype at 3 dpf. The F2 *mob*^{m610} embryos were frozen and DNA was extracted by proteinase K digestion (buffer: 10 mM Tris, 50 mM KCl, 1% Tween 20, proteinase K 1 mg/ml) overnight at 55°C followed by heat inactivation at 98°C for 10 minutes. DNA from a single embryo was diluted in 500 μl TE buffer and 5 μl were used per PCR reaction. We then pooled in equal proportions DNA of 10 *mob*^{m610} and 10 wild-type sibling embryos. The two pools were PCR-genotyped with a set of SSLP (simple sequence length polymorphism) markers evenly spaced across the zebrafish genome [on average every 20 centiMorgans (Knapik et al., 1998)] and resolved by electrophoresis on 2% agarose gels. Potential linkages were tested on individual embryos in order to define the critical interval containing the *mob*^{m610} mutation.

SSCP (single strand confirmation polymorphism) (Foernzler et al., 1998) analysis of the 3′UTR region of *tfap2a* was performed by PCR with the addition of α^{32}P-dCTP, and products were resolved in MDE (BioWhittaker) or 6% acrylamide denaturing gels run at constant voltage for 12-14 hours. After electrophoresis, gels were transferred to Whatman paper and exposed to X-OMAT film (Kodak) at –80°C without drying.

Three isoforms of *tfap2a* varying by an alternatively spliced first exon were found in public databases: *tfap2a1*, *tfap2a2* (Gene Bank Accession Numbers AF457191 and AF457192, respectively) and *tfap2a3* (zebrafish EST fc31a07). mRNA was isolated from 4 dpf embryos with the Trizol reagent (Invitrogen). Full-length cDNA cloning of *tfap2a* isoforms was performed with primers ap2a1F1 (CTCGAGCCTTGTATGCACTG), ap2a2F1 (GAGGGACACAAG-ACCCAATG), ap2a3F1 (GCATCTAAAGGGCAGACGAA) and ap2aR (TAAATGCCAAGATCGGAAGG). The PCR products were sequenced with the same primer set plus ap2aF2 CGGGTT-ACCGCATCAACTAT. RT-PCR was carried out using the Platinum Taq system (Invitrogen). Genomic DNA including the *tfap2a* exon 7 full coding region was amplified with primers ap2a-ex7F ACGG-AATACGTGTGTCATCG and ap2a-ex7R GGTGGTGGGTTCAG-TGTTTC yielding a product of 504 bp that was sequenced with the same primers. The *Xba*I restriction digest of the amplification product yielded two fragments of 378 bp and 126 bp for wild-type embryos but owing to obliteration of the *Xba*I site, the 504 bp fragment for *mob*^{m610} mutant embryos. A second *mont blanc* allele (*mob*^{m819}) was cloned that introduces a stop codon at the end of exon 5 leading to deletion of the dimerization and DNA-binding domains encoded by exons 6 and 7 (Holzschuh et al., 2003).

The full-length sequence of the *tfap2a* gene was assembled based on the genomic sequences obtained from the Sanger Institute (The *Danio rerio* Sequencing Project; http://www.sanger.ac.uk/Projects/D_rerio/).

In situ hybridization and immunohistochemistry

Whole-mount in situ hybridization was performed as described by

Thisse et al. (Thisse et al., 1993). The following probes were used: *crestin* (Rubinstein et al., 2000), *dlx2* (Akimenko et al., 1994), *dbh* (Holzschuh et al., 2003), *dct* (Kelsh et al., 2000b), *foxd3* (Kelsh et al., 2000a), *hoxb2a* (Prince, 1998), *kit* (Parichy et al., 1999), *snail2* (Thisse et al., 1995), *sox9a* (Chiang et al., 2001), *sox10* (Dutton et al., 2001), *wnt5a* (Rauch et al., 1997) and *xdh* (Parichy et al., 2000). Embryos were staged and fixed overnight in 4% PFA in PBS at 4°C, then washed in PBS/0.1% Tween 20 (PBT), dehydrated stepwise to methanol, and stored at –20°C.

For antibody staining, embryos were anesthetized and fixed overnight in 4% PFA in PBS at 4°C. After washing, they were dehydrated to methanol and stored at –20°C. After rehydration, embryos were permeabilized with proteinase K, re-fixed and washed in PTD [1% dimethylsulfoxide (DMSO), 0.3% Triton X-100 in PBS]. They were then incubated in blocking solution (PBT, 2% heat-inactivated normal goat serum, 2 mg/ml BSA). Anti-Hu antibody (Molecular Probes) was prepared in blocking solution at 1:100 dilution and anti-myosin antibody (kindly provided by Dr E. Kremmer, GSF) at 1:10 dilution of the hybridoma supernatant, and incubated overnight at 4°C. After extensive washes in PTD, embryos were incubated with biotinylated secondary antibodies (Vector) at 1:200 dilution in blocking solution for 1 hour at room temperature. The color reaction was developed using the Vectastain ABC kit with horseradish peroxidase and DAB as chromogen (Vector). After staining embryos were cleared and stored in 80% glycerol. For flat-mount preparations, yolk was removed with fine needles and embryos were mounted between cover slips. Preparations were photographed using a Zeiss Axioscope microscope and composite images were prepared with Adobe Photoshop.

Fate mapping of cranial neural crest cells

Embryos were injected at the one to two-cell stage with a 5% solution of DMNB-caged fluorescein 10,000 M_r (Molecular Probes) in 0.2 M KCl. At the 6- to 8-somite stage, the most dorsal region of the hindbrain was exposed to a 10 second light pulse from a 354 nm laser mounted on a Zeiss LSM510 inverted confocal microscope. Embryos were photographed immediately to document the extent of uncaging, allowed to develop until 24 hpf and re-photographed.

Cell death assays

TUNEL (terminal transferase mediated dUTP nick end-labeling) and Acridine Orange labeling were used to assess apoptosis in *mob*^{m610} mutants. For TUNEL analysis, embryos were staged and fixed as for in situ hybridization and stored in methanol. After rehydration, embryos were permeabilized by proteinase K digestion, re-fixed in buffered 4% PFA, washed in PBT and subsequently placed in terminal transferase buffer (Roche). Embryos were incubated on ice for 1 hour with terminal transferase (Roche) and biotin-labeled ddUTP (Roche) followed by 1 hour incubation at 37°C. Next, embryos were extensively washed in PBT and the biotin incorporation was detected with the peroxidase ABC kit (Vector) using DAB as chromogen. Embryos were stained at 10 timepoints (experiment 1: 18, 19, 20, 22, 23, 24 hpf; experiment 2: 24, 26, 28, 30, 32 hpf) to determine at which stage the cells are eliminated. In each batch, 40 embryos were obtained by mating of carrier fish, thus expecting 10 mutant and 30 wild-type embryos (n=440).

Live embryos were stained for apoptotic cells with the vital dye Acridine Orange that permeates inside acidic lysosomal vesicles and becomes fluorescent, thus marking cells dying by apoptosis. The stock solution (5 mg/ml in egg water, 300×) was diluted to 1× concentration and dechorionated embryos were bathed in this solution for 20 minutes in the dark. Embryos were washed in egg water and analyzed under a fluorescence microscope. After initial optimization of the protocol, we stained embryos obtained from mating of carrier fish at 24 to 25 hpf (n=72 from *mob*^{m610} and n=40 from *mob*^{m819}). We exposed embryos only once to UV light during photography and allowed them to develop in the dark until the visible phenotype of the *mont blanc* embryos could be scored. We detected normal apoptosis levels in the lens of both wild-type embryos and *mob* mutants that served as an internal control.

Results

Jaw defects in *mob*^{m610} mutants

The zebrafish *mob*^{m610} allele was isolated in a large-scale ENU-mutagenesis screen for embryonic patterning mutations (Driever et al., 1996; Neuhauss et al., 1996). *mob*^{m610} is inherited in a recessive fashion and the mutant phenotype segregates in Mendelian manner (25% mutants). The *mob*^{m610} mutation is characterized by visible craniofacial defects that are first observed around 2.5 dpf. The rostral tip of Meckel's cartilage in wild-type embryos is pointed dorsally and allows fish to close their mouth (Fig. 1A). In *mob*^{m610} mutant embryos, the long axis of Meckel's cartilage is pointed ventrally leading to a gaping jaw (Fig. 1B). The additional loss of posterior arches creates a chasm between the first pharyngeal arch and the edemic heart.

We have stained head cartilages with the Alcian Blue dye that binds to carbohydrate moieties of extracellular matrix proteoglycans and demarcates differentiated chondrocytes (Fig. 1C). Analysis of Alcian Blue stained preparations of *mob*^{m610} embryos revealed normally shaped cartilages of the first pharyngeal arch (Meckel's and palatoquadrate) while the second or hyoid arch derivatives (ceratohyal, hyosymplectic) were severely reduced (Fig. 1D). Posterior pharyngeal arches (3 to 7) were not detectable (zebrafish pharyngeal arches 1-7 are equivalent to branchial arches 1-7 in amniotes). We occasionally observed in mutant embryos small cartilage rods at the location where the ceratohyal and ceratobranchials are normally expected. These cartilage rods were built by cytologically normal chondrocytes that were correctly shaped and stacked. Based on their relative location with respect to the remaining head skeleton, it appears that these small remnants represent incomplete cartilages of posterior pharyngeal arches.

We did not observe any defects in mesodermally derived neurocranium cartilages in the *mob*^{m610} mutant embryos. By contrast, the trabeculae originating from neural crest and mesoderm had a normal rostral extent but failed to fuse and build the ethmoid plate. The lack of ethmoid plate shows variable penetrance (in ~40% of *mob*^{m610} mutant embryos) and expressivity (varying from complete separation of the two trabeculae to small discontinuations in the ethmoid plate of two to three cells length). This phenotype is reminiscent of clefting of the palate in higher vertebrates. The pectoral fins develop normally. These results indicate that the *mob*^{m610} mutation specifically affects the neural crest-derived craniofacial skeleton of pharyngeal arches two to seven and the neural crest derived ethmoid plate, while the first pharyngeal arch as well as the mesodermally derived neurocranium and the pectoral fins are not affected.

Dorsal pharyngeal arch muscles are absent in *mob*^{m610} mutants

As neural crest derived craniofacial cartilage is known to pattern associated head musculature (Noden, 1983; Schilling and Kimmel, 1997), we examined how the *mob*^{m610} mutation affects development of craniofacial muscles using an antibody against myosin (Fig. 1E). Our analysis revealed that the

adductor mandibulae (am), a dorsal muscle originating from the first arch territory, is always present as are all ventral muscles of the first arch, the intermandibularis anterior (ima) and intermandibularis posterior (imp) (Fig. 1F). The latter muscle is displaying a varying degree of deformity ranging from slight elongation to shorter and defasciculated fibers joining caudally with second arch muscles. By contrast, the two dorsal muscle pairs of the mandibular arch, levator arcus palatini (lap) and dilator operculi (do) are absent in *mob* mutants (Fig. 1G,H). Similarly, the dorsal hyoid arch muscles, the adductor opercule (ao), the levator operculae (lo) and the adductor hyomandibulae (ah) are also absent in *mob*^{m610} mutant embryos (Fig. 1G,H). The ventral muscles of the second pharyngeal arch, interhyals (ih) and hyohyals (hh) are hard to distinguish as individual muscles, but all mutants have a bundle of muscle fibers in the approximate location of the ih and hh.

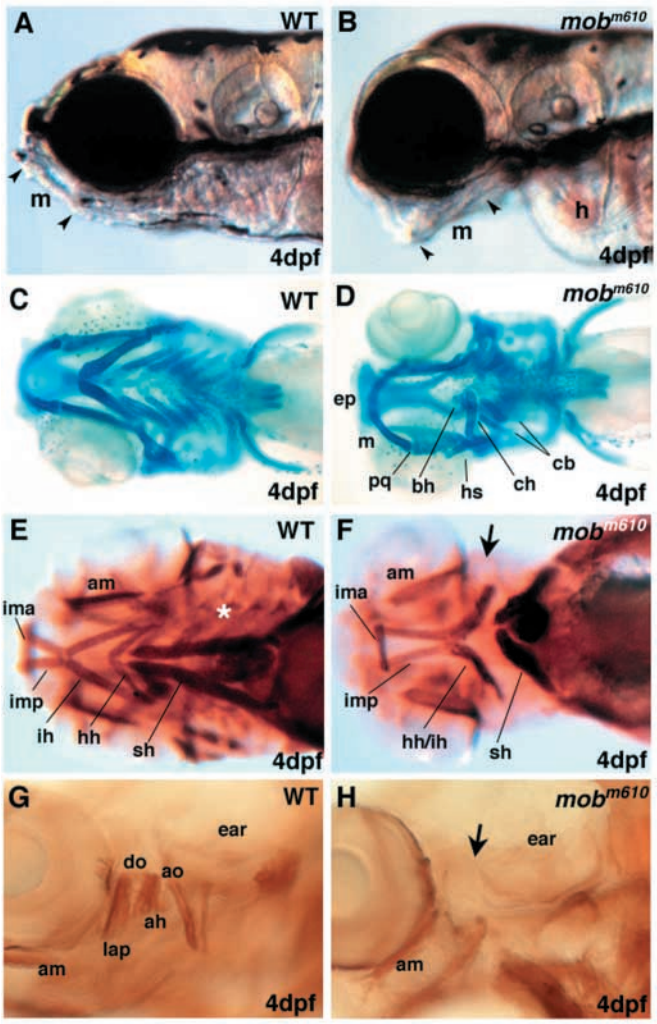

Fig. 1. The *mont blanc* (*mob*^{m610}) mutation affects zebrafish craniofacial development. (A,B) Lateral view of wild-type (A) and *mob*^{m610} (B) live embryos at 4 dpf. In *mob*^{m610} embryos the Meckel's cartilage is pointing ventrally and the posterior arches are missing (arrowheads point to the anterior and posterior tips of the Meckel's cartilage). The heart develops an edema. (C,D) Ventral view of Alcian Blue stained heads visualizes the craniofacial skeleton of wild-type (C) and *mob*^{m610} (D) embryos at 4 dpf. Cartilage elements corresponding to second and posterior arches are severely reduced. bh, basihyal; cb, ceratobranchial; ch, ceratohyal; ep, ethmoid plate; h, heart; hs, hyosymplectic; m, Meckel's cartilage; pq, palatoquadrate. (E,G) Wild-type and (F,H) *mob*^{m610} embryos at 4 dpf. (E,F) Ventral view of cranial musculature; muscles of second and posterior arches are disorganized in the mutant. The asterisk marks the area of ceratobranchial muscles. (G,H) At higher magnification, a lateral view of the head reveals that a number of dorsal muscles are missing in mutant embryos (arrow in F,H). ah, adductor hyomandibulae; am, anterior mandibularis; ao, adductor opercule; do, dilator operculi; hh, hyohyoideus; ih, interhyoideus; ima, intermandibularis anterioris; imp, intermandibularis posterioris; lap, levator arcus palatini; sh, sternohyoideus.

The individual posterior pharyngeal arches 3 to 7 have their own set of small muscles for each of the paired ceratobranchial cartilages, i.e. the transversi ventrales, rectus ventralis, dorsal pharyngeal wall muscles and rectus communis. We were not able to identify symmetric sets of muscles in *mob*^{m610} mutants as found in wild-type embryos, although small clusters of myosin positive cells were occasionally seen in the last posterior arch in some of the mutant embryos. The most superficially located muscle, sternohyoideus (sh), stretching from the pectoral girdle cartilages to the ceratohyal cartilage, is always present in *mob*^{m610} mutants but is shorter and thicker conserving its caudal attachment, while rostrally extending only to the anterior edge of the heart. It is interesting to note that all eye movement muscles are well formed and positioned in *mob*^{m610} (not shown). Our findings indicate that loss of craniofacial cartilage elements is accompanied by loss of the corresponding muscle sets in the *mob*^{m610} mutant embryos.

Molecular nature of the *mob*^{m610} mutation

To identify the affected gene, we genetically mapped the *mob*^{m610} mutation and used a positional candidate cloning strategy. Genotyping of wild-type and *mob*^{m610} mutant pools of DNA from F2 animals with SSLP markers (Knapik et al., 1998) linked *mob*^{m610} to LG24. Linkage was confirmed by genotyping of individual F2 mutant embryos with the flanking markers Z59948 and Z15002. Using over 3400 meioses we established a fine map of the region and were able to restrict the critical genetic interval harboring the *mob*^{m610} mutation between markers Z23011 (1.3 cM, 39 recombinants out of 2930 meioses) and Z65547 (1.1 cM, 39 recombinants out of 3356 meioses; Fig. 2A). Considering the relatively large genetic interval of 2.3 cM (approximately 1.5 Mb), we examined available human and mouse synteny maps, as well as zebrafish ESTs mapped on the radiation hybrid panels (www.zfin.org), to search for positional candidate genes. The most plausible candidate appeared to be the transcription factor ap-2α. Tcfap2a is expressed in neural crest progenitor cells (Mitchell et al., 1991) and mice lacking functional *Tcfap2a* exhibit craniofacial defects, hypoplastic heart and kidneys, and have strong reduction of neural crest derived peripheral neurons (Zhang et al., 1996; Schorle et al., 1996). To test whether *tfap2a* is disrupted in *mob*^{m610}, we developed a set of PCR primers revealing a polymorphism in the 3′UTR of the gene. Using SSCP analysis we genotyped all 78 meiotic recombinants flanking the mutation and did not find a single recombination event between the *mob* locus and the *tfap2a* gene. The very close linkage of less than 0.03 cM (<20 kb) provided the first indication that the *mob* locus corresponds to the *tfap2a* gene.

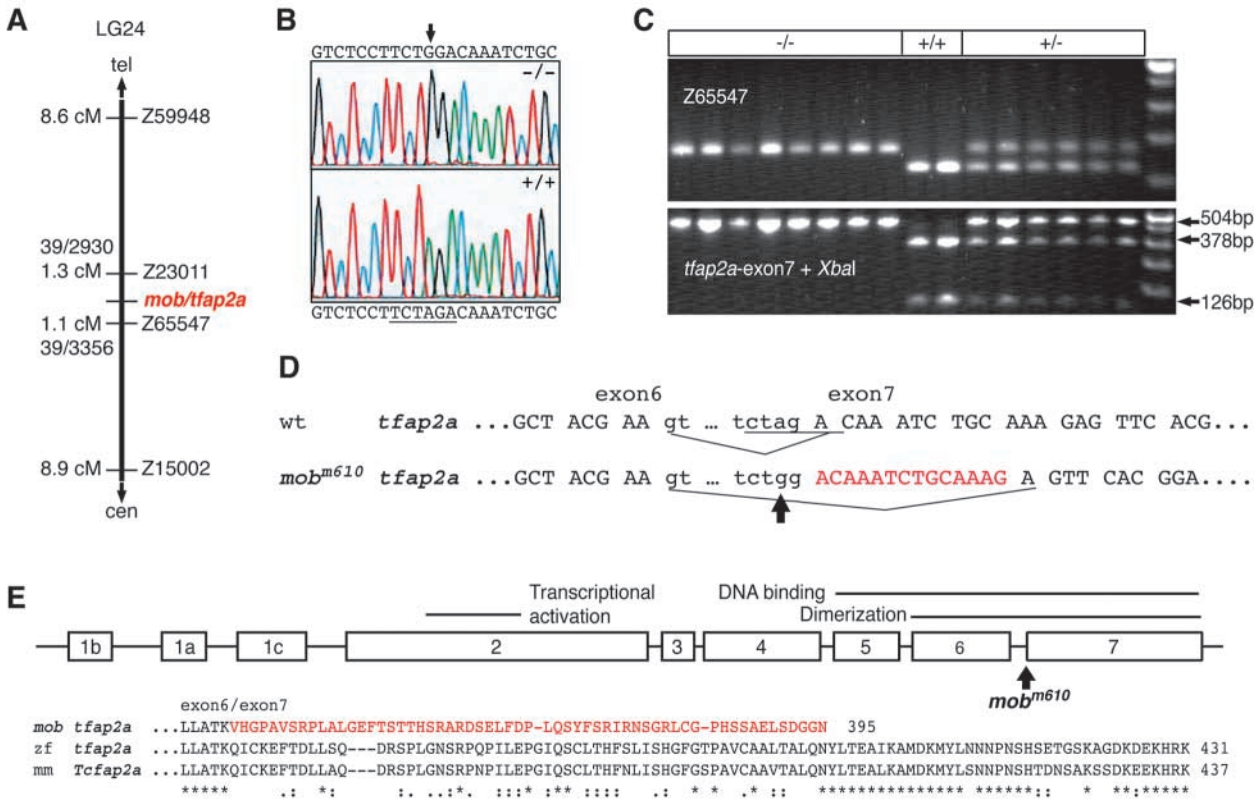

Fig. 2. *mont blanc* encodes *tfap2a*. (A) *mob*^{m610} maps on linkage group 24, between markers Z23011 and Z65547. No recombinants were found between *mob*^{m610} and a SSCP marker in the 3′UTR of *tfap2a*. (B) Genomic sequence of wild-type and *mob*^{m610} embryonic DNA reveals an A→G transition (arrow) at the 3′splice site preceding exon 7 in the mutant. (C) Mutation in the *Xba*I site (underlined in B and D) is tightly linked to the *mob*^{m610} phenotype. Upper panel shows a sample of map cross animals genotyped with SSLP marker Z65547. In lower panel, DNA from the same animals is amplified and digested by the *Xba*I enzyme. PCR products spanning the *mob*^{m610} lesion are not cut. (D) Sequence of wild-type and mutant *tfap2a* cDNA (in capital letters) reveals a 14 bp deletion (in red) that corresponds to the beginning of exon 7. Part of intron 6 is also depicted (in small letters). The *Xba*I site destroyed by the mutation is underlined and the arrow indicates the mutated base pair. (E) Genomic structure of the *tfap2a* gene. Exon 1a corresponds to isoform *tfap2a1*, exon 1b to *tfap2a2* and exon 1c to *tfap2a3*. The arrow indicates the mutation site at the 3′splice site of intron 6. Sequence homology alignment between the C-terminal part of the protein in *mob*^{m610} mutants, wild-type zebrafish and mouse *Tcfap2a* that shares 86% homology with the zebrafish *tfap2a*. The usage of the cryptic 3′splice site within exon 7 produces a reading frame shift and disrupts the C-terminal part of the protein. The predicted missense peptide (in red) shares little sequence similarity with the wild-type sequence that is responsible for dimerization and DNA binding of *tfap2a*.

To verify this notion, we cloned and sequenced the corresponding genomic DNA fragment from homozygote *mob*^{m610} embryos and compared it with the sequence from wild-type and heterozygote siblings. We found a single nucleotide A→G transition between *mob*^{m610} and wild-type animals, a change often seen in ENU-induced mutations (Knapik, 2000), in the sequence of intron 6 at the splice junction area (Fig. 2B). This mutation destroys an *Xba*I restriction endonuclease recognition site allowing identification of the *mob*^{m610} mutants in a PCR/RFLP (restriction fragment length polymorphism) assay (Fig. 2C). To confirm the splice variant, we cloned and sequenced the full-length cDNA of the *tfap2a* gene and found a 14 bp deletion in the cDNA of mutant embryos that was common to all three *tfap2a* isoforms (Fig. 2D). The *mob*^{m610} mutation abolishes the 3′ splice junction and forces the splicing machinery to use a cryptic site within exon 7 leading to a deletion of 14 bp and a frame-shift in the resulting C terminus of the protein (Fig. 2E). We were interested whether the splicing machinery may produce a small amount of wild-type message in the mutant background. To test this possibility, we amplified cDNA fragments spanning the mutation and deletion sites by RT-PCR from wild-type and mutant embryos, and digested them with the *Hpy CH4V* restriction endonuclease (recognition site located within the 14 bp deletion; data not shown). In contrast to wild-type controls, we did not obtain any digested fragments from the RT-PCR products originating from *mob*^{m610} mutant embryo cDNA. Therefore, at the sensitivity of the RT-PCR assay, there appears to be no correctly spliced message in *mob*^{m610} mutants. Our data indicate that the *mob*^{m610} mutation results in an ablation of the exon 7 encoded part of the Tfap2a protein. cDNA sequencing data showed that *mob*^{m610}*/tfap2a* is correctly translated up to Lys 336 followed by a missense peptide of 33 amino acids and a premature stop codon truncating the protein 36 residues short of its normal length (Fig. 2E). The mutant protein has no resemblance to its wild-type counterpart in the C terminus, and does not match any sequences in available databases. This protein domain is responsible for dimerization and DNA binding and thus is absolutely necessary for the transcriptional activity of TFAP2A

(Williams and Tjian, 1991a; Williams and Tjian, 1991b). Our findings strongly suggest that the mutation in *mob*^{m610} leads to a complete loss-of-function of the *tfap2a* gene.

tfap2a is expressed in neural crest progenitors, pronephric ducts and brain

The *tfap2a* gene is broadly expressed as early as 50% epiboly (Fig. 3A) and as development progresses, it becomes restricted to the neural plate border. At the 2-somite stage *tfap2a* is found in the neural crest progenitor cells (Fig. 3B,C). This expression domain is maintained as the cranial neural crest cells begin to migrate by the 10-somite stage (Fig. 3D,E). At 14-somite stage, expression commences in the intermediate mesoderm in the caudal part of the embryo (Fig. 3F,G). At this time, expression continues in migrating cranial neural crest cells and premigratory trunk neural crest cells (Fig. 3F,G). In parallel, the *tfap2a* transcript appears in the midbrain, hindbrain and spinal cord (Fig. 3F,G). About 2 hours later, the number of cells expressing *tfap2a* has increased and now it can be also seen in the epidermis and developing pronephric ducts (Fig. 3H,I). At 24 hpf, the craniofacial primordia continue to express *tfap2a*. In addition, the lateral line primordium, several sites in the hindbrain, the cerebellum, the tectum and the epiphysis stain positive for *tfap2a* (Fig. 3J,K). The expression in pronephric ducts is downregulated at this stage. At 36 hpf, *tfap2a* expression is observed in the segmented hindbrain rhombomeres, in the pharyngeal arches and in a group of cells positioned between the otic vesicle and the pharyngeal arches that will give rise to the epibranchial ganglia (Fig. 3L). Expression analysis in embryos obtained from mating of *mob*^{m610} carrier fish did not reveal any differences in the levels of the *tfap2a* message between wild-type and mutant animals, indicating that this gene is not autoregulated.

mob^{m610} is required for development of pigment cells

The earliest phenotype detectable in *mob*^{m610} mutants is a severe reduction of head and trunk pigmentation, clearly recognizable at 36 hpf (Fig. 4A,B). At this time, single melanophores (melanin producing pigment cells) are present in the head region of *mob*^{m610} mutants (anterior to the otic capsule; Fig. 4B). In the trunk, melanophores are present in the dorsal and lateral stripes with few cells reaching the ventral stripe. No cells are found spreading over the yolk sac, while at the same time the melanophores are already present over the yolk extension in wild-type embryos (Fig. 4A,B). The dorsoventral as well as the anteroposterior extent of melanophore pigmentation is clearly diminished in *mob*^{m610} mutants, indicating that at equivalent developmental stages the dorsoventral migration of melanophores is less advanced. At the stage when melanophores have reached the tip of the tail

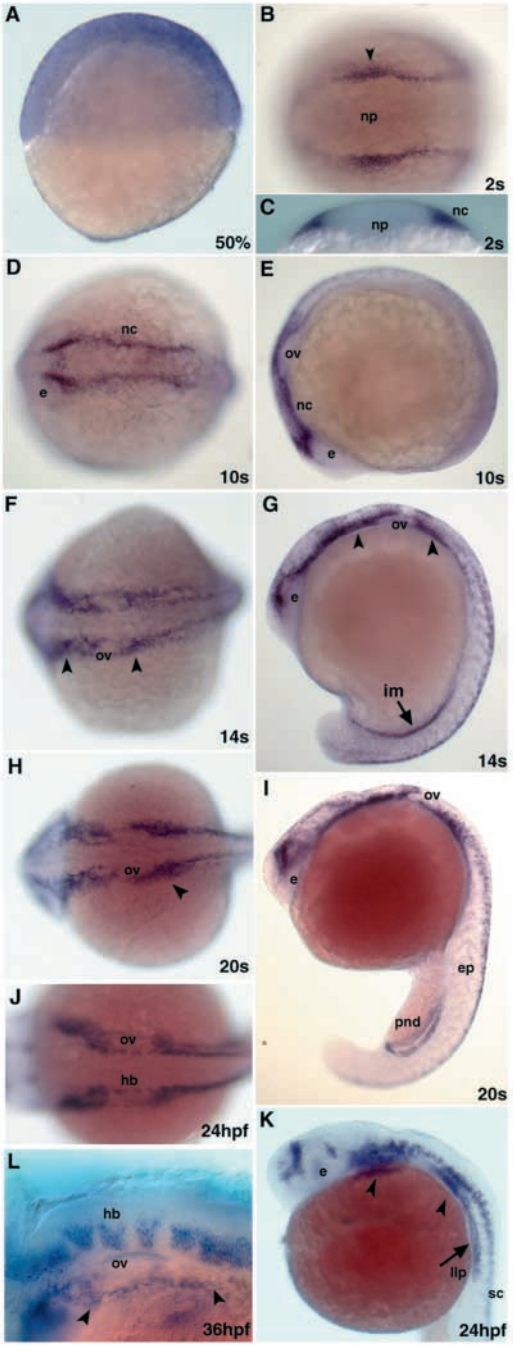

Fig. 3. Embryonic expression of *tfap2a*. (A,E,G,I,K) Lateral and (B,D,F,H,J) dorsal views of embryos stained with a *tfap2a* riboprobe (B,D-K, anterior is towards the left). (A) Expression at 50% epiboly is spread throughout the blastoderm with a slightly stronger expression at the most dorsal aspect of the embryo. (B,C) *tfap2a* expression in neural crest progenitors at the two-somite stage. Arrowhead in B indicates the level where the optical section was taken in C. (D,E) Cranial premigratory neural crest cells express *tfap2a* at the 10-somite stage. (F,G) Expression extends to migratory neural crest cells (arrowheads), intermediate mesoderm, brain and spinal cord neurons. (H,I) *tfap2a* message is found in brain and spinal cord neurons, neural crest streams in the head (arrowhead), in the epidermis and the paired pronephric ducts. (J,K) At 24 hpf, the expression in the brain is confined to the two anterior domains and the hindbrain rhombomeres. At this time, increasing numbers of spinal cord neurons and the migrating lateral line primordium (arrow) express *tfap2a*. Arrowheads indicate the craniofacial primordia. (L) Dorsolateral view of the head at 36 hpf. The expression in the primordia of the epibranchial ganglia is visible as a stripe of cells (arrowheads) between the otic vesicle and the pharyngeal arches. e, eye; ep, epidermis; hb, hindbrain rhombomeres; im, intermediate mesoderm; llp, lateral line primordium; nc, neural crest; np, neural plate; ov, otic vesicle; pnd, pronephric ducts; sc, spinal cord neurons.

in wild-type embryos, in mutant fish the caudal migration wave extends only up to two-thirds in the anterior trunk and tail, leaving the most posterior one third devoid of melanophores. This picture changes at 48 hpf when the number of melanophores has increased and their anteroposterior and dorsoventral range more closely resembles the pattern seen in wild-type embryos (Fig. 4C,D). A small patch of melanophores covers the back of the head and individual cells are flattened with symmetrical morphology typical to post-migratory cells. Consistently, the melanophores in the *mob*^{m610} mutants neither reach the tip of the tail nor do they migrate around it, and very few cells are found in the lateral and ventral stripes in the caudal one third of the embryo.

Unlike the melanophores, the iridophores are almost absent in *mob*^{m610} mutant embryos (Fig. 4E,F). We have counted the number of iridophores in mutant embryos and found that one third of them lack iridophores at 4 dpf, while the remaining two-thirds have only a few iridophores (one to eight) posterior to the ear.

To investigate at what stage of pigment cell development tfap2a functions, we analyzed mRNA expression of *dct* (*dopachrome tautomerase*), a marker of unpigmented melanoblasts and pigmented melanophores (Kelsh et al., 2000b). In wild-type embryos at 22 hpf, *dct*-labeled melanoblasts in the head are concentrated in a cluster posterior to the eye, while the trunk melanoblasts are mostly located at the post-otic region and begin to disperse over the yolk sac moving in ventroposterior directions (Fig. 4G). In *mob*^{m610} mutants, there are very few melanoblasts posterior to the eye and a small cluster of cells in the region posterior to the ear with only sporadic cells migrating over the yolk sac (Fig. 4H). Expression of the *mitfa* transcription factor, a key gene in melanoblasts specification, is only slightly delayed in mutant embryos (data not shown) but the tyrosine kinase receptor *kit* that labels the differentiating pigment cell lineage is dramatically reduced in melanoblast (Fig. 4I,J).

The development of xanthophores, the third pigment cell type in zebrafish, is also affected by the *mob*^{m610} mutation. Xanthophore migratory progenitors can be identified by *xanthine dehydrogenase* (*xdh*) expression, one of the enzymes in the xanthopterin synthesis pathway. We found that *xdh* expression is markedly diminished in the anterior trunk of 25 hpf *mob*^{m610} mutant embryos, but a sizable population of migrating cells is present in the posterior trunk (Fig. 4K,L). Xanthophores appear normal at 48 hpf (Fig. 4C,D) giving embryos the characteristic golden hue that intensifies as development progresses.

Taken together, our results suggest that normal development of pigment cells depends on *tfap2a* function, as shown by deficits in the melanization and the diminished expression of early markers defining neural crest derived pigment cells.

Satellite cell glia, dorsolateral placodes and epibranchial ganglia require *tfap2a/mob* for normal development

In zebrafish, progenitor cells that will differentiate into satellite cells associated with cranial ganglia neurons express *foxd3* (Kelsh et al., 2000a). We analyzed *foxd3* expression in 24 hpf embryos to determine if *tfap2a* is necessary for patterning and differentiation of the neural crest derived glial lineage (Fig. 5A). At this stage, we found a severe reduction but not absence of *foxd3* expression in cells surrounding cranial ganglia. This effect was most pronounced in the trigeminal ganglion and the ganglia that occupy the preotic region (Fig. 5B). The reduction of expression was least evident in ganglia located posterior to the otic vesicle.

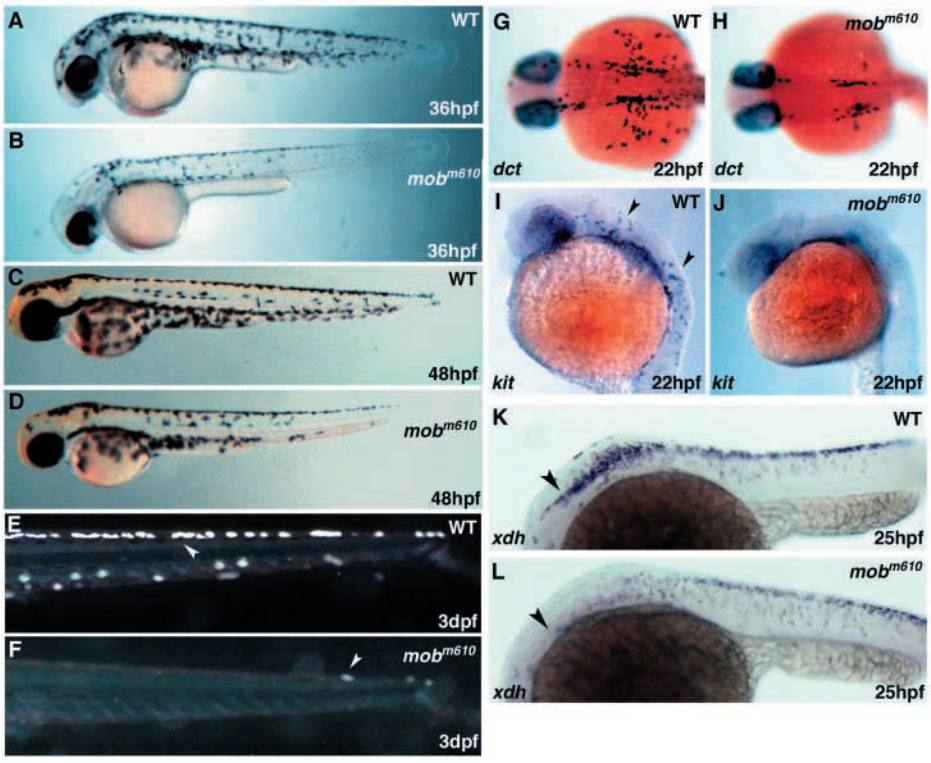

Fig. 4. Abnormal pigmentation in *mob*^{m610} mutant embryos. (A,B) Wild-type (A) and *mob*^{m610} (B) live embryos at 36 hpf. Pigmentation is reduced in a *mob*^{m610} embryo, with melanophores missing in the head and in the tail. (C,D) Wild-type (C) and *mob*^{m610} (D) live embryos at 48 hpf. The defect in pigment cell distribution is still visible in the distal part of the tail, but less evident than at earlier stages. (E,F) Development of iridophores is severely affected in *mob*^{m610} embryos. Iridophores (indicated by arrowheads) in the tail were photographed under incident light at 3 dpf in wild-type (E) and *mob*^{m610} (F) embryos. (G,H) Expression of *dopachrome tautomerase* (*dct*) at 22 hpf in wild-type (G) and *mob*^{m610} (H) embryos. (I,J) Expression of *kit* tyrosine kinase receptor at 22 hpf in wild-type (I) and *mob*^{m610} (J) embryos. Arrowheads indicate migrating pigment cell precursors. (K,L) Expression of the *xanthine dehydrogenase* (*xdh*) gene in xanthophore precursors at 25 hpf in wild-type (K) and *mob*^{m610} (L) embryos (arrowheads indicate the posterior end of the otic vesicle).

Mouse *Tcfap2*a knockout embryos display a severe reduction of neurons in cranial ganglia, especially in oculomotor (III) as well as in trigeminal (V), facial (VII), statoacoustic (VIII), glossopharyngeal (IX) and vagal (X) ganglia (Zhang et al., 1996; Schorle et al., 1996). To further explore formation of cranial ganglia, we examined the expression of *neurod* that marks all neurogenic placodes (Fig. 5C) (Andermann et al., 2002). We found that at 24 hpf the *neurod* expression domains were greatly reduced in the area of the trigeminal ganglion and in all lateral line placodes of *mob*^{m610} mutant embryos (Fig. 5D). However, in most embryos we were able to detect a few individual cells expressing *neurod*. The octaval placode expression was only slightly reduced in *mob*^{m610} mutant when compared with wild types. These results suggest that *tfap2*a function is necessary for expression of *neurod* in the trigeminal placode and in all mechanosensory (dorsolateral) placodes.

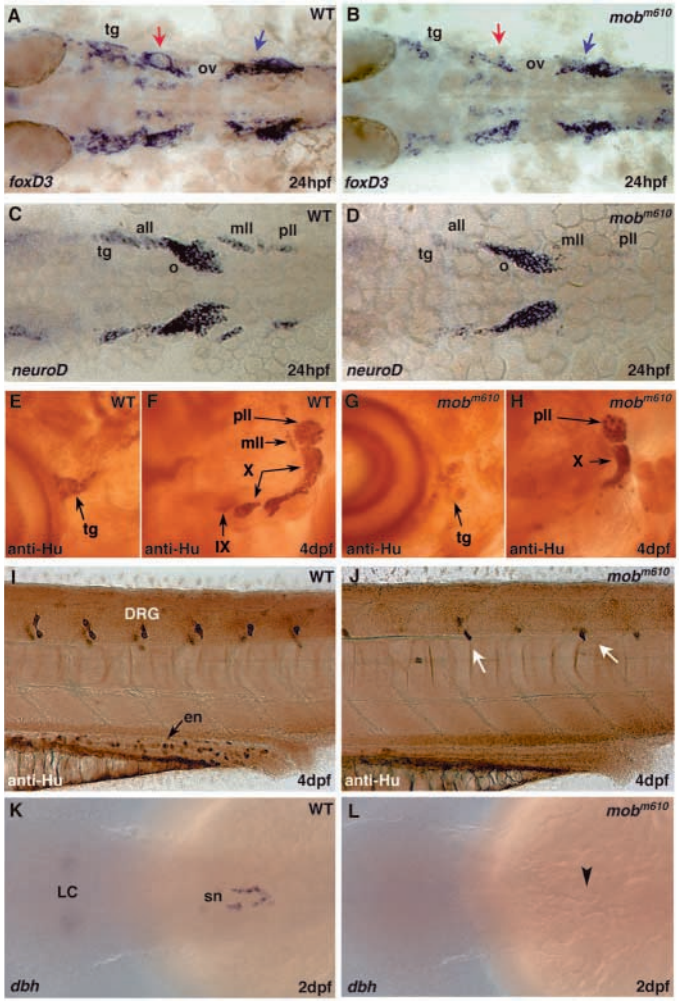

Fig. 5. Neural derivatives of neural crest require *tfap2a* activity. (A,C,E,F,I,K) Wild-type and (B,D,G,H,J,L) *mob*^{m610} embryos. (A,B) *foxd3* expression in cranial ganglia-associated glia at 24 hpf. The red arrow indicates the preotic ganglia and the blue arrow the postotic ones. (C,D) *neurod* expression in cranial ganglia precursors at 24 hpf. (E-H) Anti-Hu antibody staining of cranial ganglia at 4 dpf. In E and G, the arrow (tg) points to the most anterior cluster of trigeminal/facial/anterior lateral line ganglia that are greatly reduced in the mutants (G). The images in F and H focus on the posterior ganglia and show loss of mll and ventral ganglia. (I,J) Anti-Hu staining in the trunk of 4 dpf embryos shows scattered DRGs (arrows) and absence of enteric neurons in the distal part of the digestive tube in *mob*^{m610} embryos (DRGs from the other side of the embryo also show-through in wild-type and mutant embryos). (K,L) The expression of the *dopamine beta hydroxylase* (*dbh*) gene in sympathetic neurons (sn) is completely missing in *mob*^{m610} mutant embryos at 48 hpf (arrowhead in L). all, anterior lateral line ganglia; DRG, dorsal root ganglia; en, enteric neurons; LC, locus coeruleus; mll, medial lateral line ganglia; o, octaval/statoacustic ganglia; ov, otic vesicle; pll, posteriolateral line ganglia; sn, sympathetic neurons; tg, trigeminal ganglia; IX, glossopharyngeal nerve ganglia; X, vagal nerve ganglia.

To compare requirements for *tfap2a* function between lower and higher vertebrates, we analyzed the expression of a pan-neuronal marker to visualize the arrangement of cranial ganglia around the otic capsule at 4 dpf *mob*^{m610} embryos (anti-Hu, antibody staining, Fig. 5E-H). The most anterior cluster of cells belonging to the group of the trigeminal (tg), facial and anterior lateral line (all) ganglia appears to be reduced in size, although we have noticed variability in the severity of this phenotype ranging from slight reduction in size to a small, scattered pool of cells (Fig. 5E,G). The posterior lateral line ganglion (pll) at the caudal edge of the otic capsule appears to be unaffected, while the middle lateral line ganglion (mll) is reduced and in some cases absent. Curving around the otic capsule are clusters of cells belonging to nuclei of the vagal ganglion. It appears that the most posterior nucleus is not affected or only slightly reduced, while the middle one is in most cases absent and the anterior thickening of the vagal ganglion is significantly smaller. The glossopharyngeal ganglion positioned below the junction of anterior and ventral walls of the otic capsule as well as the octaval ganglion directly above it are practically absent with only a few cells present in some of the mutant animals (Fig. 5F,H). We obtained similar results analyzing the *ret* expression pattern by whole-mount in situ hybridization (data not shown). In summary, development of the cranial neuronal and glial lineages that are derived from neural crest and ectodermal placodes depends on *tfap2a* activity. In its absence, these cells fail to express *foxd3* and *neurod* and ultimately do not form the majority of the mechanosensory and visceral sensory cranial ganglia.

Reduction of the neural crest derived enteric nervous system and trunk sensory neurons in *mob*^{m610} mutants

Aside from pigment cells, the trunk neural crest gives rise to the peripheral nervous system. We have used the anti-Hu pan-neuronal antibody to examine the pattern of trunk dorsal root ganglia and enteric neurons in *mob*^{m610} mutant embryos. In wild-type larvae the sensory neurons of dorsal root ganglia (DRG) are distributed bilaterally along the anteroposterior (AP) axis and are positioned at the level of the ventral spinal cord with one pair of DRGs in each somitic segment (Fig. 5I). In *mob*^{m610} mutants the number of DRGs is greatly reduced. To quantify the extent of missing ganglia, we have unilaterally counted the DRGs in wild-type embryos at 4 dpf between the otic capsule and the anus. We distinguished 17 DRGs in wild-type embryos while in the *mob*^{m610} mutants there were only 5±2 (n=72) ganglia in the corresponding region (Fig. 5J) representing a ~70% reduction of normal numbers. We did not observe any region of preferential loss of ganglia along the AP

axis or in the left versus right side. At 4.5 dpf, wild-type DRGs consist of approximately three to five cells per ganglion, and the number increases with progressing development. We found that most ganglia in *mob*^{m610} mutants had the number of cells reduced by half, and many contained only one or two cells. Additionally, we observed in each embryo one or two neurons that were ectopically located at the level of notochord or dorsal neural tube.

Enteric neurons populate the gut of the larvae and at 4 dpf there are ~200 single cells distributed along the entire length of the gut (Kelsh and Eisen, 2000). Staining with anti-Hu antibody visualizes enteric neurons in wild-type embryos while most of the *mob*^{m610} mutants were devoid of enteric neurons in the distal part of the gut tube (Fig. 5I,J). In few *mob*^{m610} mutants (~32%), we observed sporadic enteric neurons in the proximal gut. Sympathetic ganglia that are of neural crest origin and will differentiate to produce noradrenergic neurotransmitters begin to express *dopamine beta hydroxylase* (*dbh*), one of the enzymes in the neurotransmitter synthesis pathway. We labeled sympathetic neurons at 48 hpf and found that there is no expression of *dbh* in *mob*^{m610} mutant embryos (Fig. 5K,L). These findings indicate that *tfap2a* is necessary for normal patterning and cell numbers of the trunk DRGs, sympathetic ganglia and enteric neurons.

tfap2a is not required for neural crest progenitors specification but is essential for activation of genetic programs that define chondrogenic neural crest

Neural crest progenitors are induced during gastrulation at the neural plate border and begin to separate from other neuronal cell types in this territory by expressing neural crest specific genes. Among the earliest genes expressed during initial stages of neural crest specification are *snail2*, *foxd3*, *sox10* and *tfap2a*. We studied expression patterns of these genes to assay neural crest specification in *mob*^{m610} mutants when compared with wild-type embryos. In *mob*^{m610} mutant embryos, we did not observe reduced expression of these genes at 1- to 10-somite stages (9 hpf through 14 hpf), the time before the onset of migration (Fig. 6A-C). Additionally, we followed the expression of *sox10*, a transcription factor characteristic for all non-ectomesenchymal neural crest progenitor cells (Dutton et al., 2001), which appears normal through the 20-somite stage in *mob*^{m610} mutants (Fig. 6D). Surprisingly, in *mob*^{m610} mutants we observed a complete loss of *crestin* expression in cranial neural crest cells at 10- and 20-somite stages and a reduction in the trunk crest (Fig. 6F,H). *crestin* is a multiple copy retro-element expressed in premigratory and migratory neural crest cells (Rubinstein et al., 2000) (Fig. 6E,H).

We noted that almost a quarter of the analyzed embryos were slightly delayed in convergence towards the midline of the two stripe-like domains of neural crest cells as revealed by in situ hybridization at 12 hpf using probes specific for the *msxc*, *snail2* and *pax3* genes (data not shown). However, staining with *hoxa2*, *hoxb2* and *hoxb3* at 10- and 20-somite stages did not show any differences in the anteroposterior extent and width of hindbrain rhombomeres (data not shown). This indicates that loss of *tfap2a* function does not lead to aberrant patterning of the neural tube and subsequent defects in induction of the neural crest.

The neural crest cells begin migration at ~15 hpf in a wave

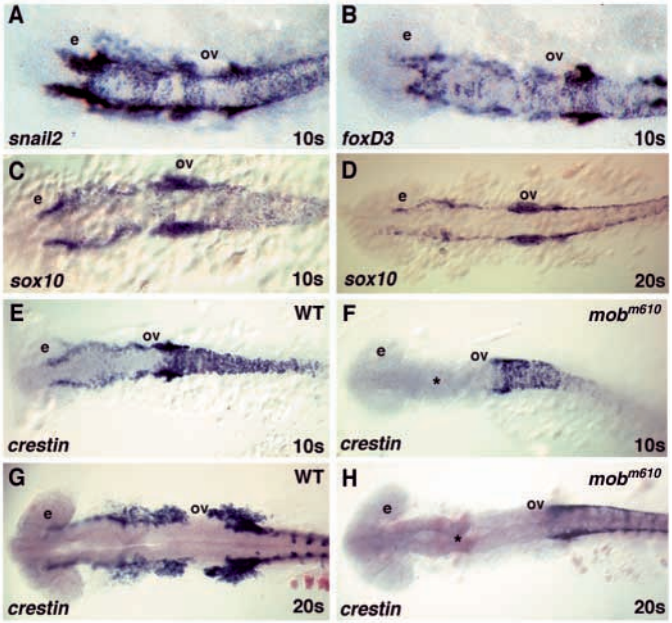

Fig. 6. Normal specification of neural crest progenitor cells in *mob*^{m610} embryos. (A,B) In situ hybridization analysis of *snail2* (A) and *foxd3* (B) expression. The patterns are indistinguishable between wild-type and *mob*^{m610} embryos at 10-somite stage. (C,D) *sox10* expression at 10- (C) and 20- (D) somite stages is also indistinguishable between wild-type and *mob*^{m610} embryos (A-D; wild-type controls not shown). (E,H) *crestin* expression in wild-type (E,G) and *mob*^{m610} embryos (F,H) at 10- (E,F) and 20-somite stages (G,H). Expression of *crestin* is completely absent in the head (asterisk) of *mob*^{m610} embryos and reduced in the trunk. All panels show dorsal views of flat-mount preparations, anterior to the left. The eye (e) and otic vesicle (ov) are marked for orientation.

originating at the midbrain and progressing along in caudal direction. At 18 hpf, the majority of chondrogenic neural crest cells begin descending towards the pharyngeal arches, while the trunk neural crest is just starting to enter the medial migratory pathway. The neural crest migration continues through 24 hpf. Considering that *mob*^{m610} mutants are deprived of chondrogenic derivatives, while initially neural crest cells appear to be specified normally, we tried to identify the time when chondrogenic precursors are eliminated. As mentioned above, analysis of migratory neural crest showed that expression of *hoxa2*, *hoxb2* and *hoxb3* at 18 hpf is normal in the rhombomeres and migrating neural crest in *mob*^{m610} embryos. By contrast, at 24 hpf Hox genes were not expressed in the second and postotic neural crest streams, while their hindbrain expression was unaffected (Fig. 7C,D and data not shown). Similarly, the expression of *dlx2*, *sox9a* and *wnt5a* was only slightly reduced in *mob*^{m610} embryos at 18 hpf, and at 24 hpf we found normally demarcated first stream of neural crest carrying cells to the mandibular arch. However at this stage, in *mob*^{m610} embryos we could not detect the second neural crest stream entering the hyoid arch and the postotic crest supplying posterior pharyngeal arches (Fig. 7A,B,E-H). In some mutant embryos, we found a few cells expressing neural crest specific genes in the migratory paths of the posterior pharyngeal arches. Taken together, our data suggest that *tfap2a* is not acting during the neural crest specification phase, but rather is needed later

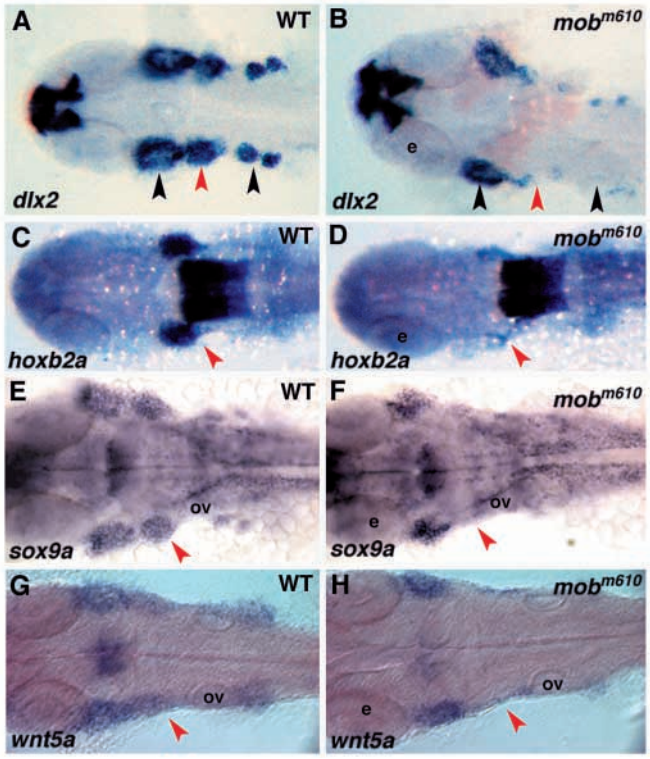

Fig. 7. *mob*^{m610} mutant embryos fail to express pre-chondrogenic genes in cranial neural crest streams populating the pharyngeal arches. (A,C,E,G) Wild-type and (B,D,F,H) *mob*^{m610} mutant embryos at 24 hpf. (A-D) In situ hybridization analysis of *dlx2* (A,B) and *hoxb2a* expression (C,D). Note normal expression of *hoxb2a* in hindbrain rhombomeres 3 to 5. (E-H) In situ hybridization analysis of *sox9a* (E,F) and *wnt5a* (G,H). The red arrowheads indicate the second neural crest stream and the black ones the first and postotic streams. All panels show dorsal views of flat-mount preparations, anterior towards the left. e, eye; ov, otic vesicle.

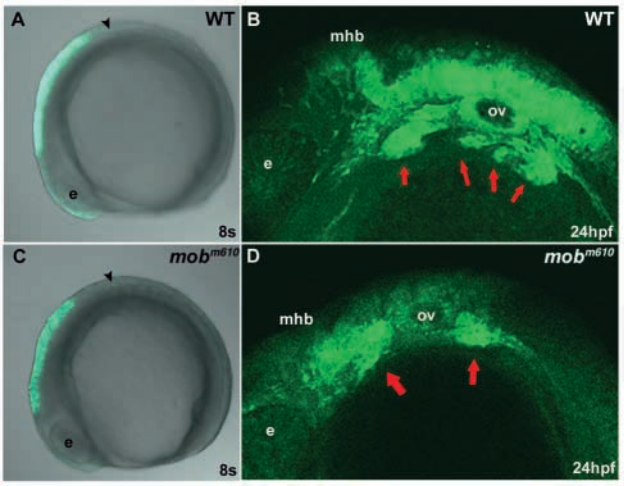

Fig. 8. Fate mapping of cranial neural crest. (A,C) Confocal microscope images of 8-somite stage embryos depict the region of UV-laser uncaged fluorescein dextran in the dorsal hindbrain. The arrowheads point to the first somite. (B,D) Confocal microscope images of the same animals as shown in A and C at 24 hpf reveal the fate of migratory neural crest in wild-type (B) and *mob*^{m610} mutant (D) embryos. In the mutant embryo, the third stream of migratory neural crest fails to subdivide and populate the most posterior pharyngeal arches. Arrows indicate the normal migrating streams towards the pharyngeal arches in wild-type embryo (B) and to the masses of premigratory cells stuck at the position of the preotic and postotic streams in *mob*^{m610} mutant (D). Lateral views. ov, otic vesicle; e, eye; mhb, midbrain-hindbrain boundary.

to maintain neural crest proliferation, identity, and/or differentiation.

Cranial neural crest cells migrate in the mandibular stream to the first arch but fail to assemble hyoid and postotic streams in the absence of *tfap2a*

Molecular analysis of neural crest progenitors, migratory populations and specific derivatives revealed that loss of *tfap2a* function has no effect on early neural crest induction and probably has no effect on neural crest cell specification. We found evidence that loss of *tfap2a* function disrupts the gene expression in the streaming cranial neural crest that is first detectable at 18 hpf, and leads to almost complete loss of expression of chondrogenic neural crest markers by 24 hpf. These results posed a question whether the loss of gene expression was due to downregulation of specific factors or to the physical paucity of migratory neural crest cells.

To address this issue, we traced the fate of neural crest progenitors in live embryos. We labeled embryos from a cross of heterozygous *mob*^{m610} parents by injecting caged fluorescein into one- or two-cell stage embryos. These animals were allowed to develop until the 6- to 8-somite stage when the dorsal edge of the hindbrain was exposed to UV-laser light to uncage the fluorescein in the territory from which neural crest progenitors will begin to migrate (Fig. 8A,C). Every embryo (n=20 in each of two independent experiments) was photographed and individually tracked until 24 to 25.5 hpf when we analyzed the migration of craniofacial primordia. We found that in 29 animals migrating neural crest was separated into individual streams (Fig. 8B). In the remaining nine animals (two embryos died) we observed migrating cells of the first pharyngeal arch, while the pre-otic and post-otic streams never left the level of the ventral margin of the neural tube. There the cells clustered together as an amorphic mass (Fig. 8D). In some of these animals, we noted individual or very small groups of cells leaving the neural tube and migrating in ventral direction. All experimental animals were allowed to develop up to 3 dpf when they were scored for the morphological *mob*^{m610} phenotype. All embryos in which preotic and postotic neural crest streams failed to migrate developed the characteristic *mob*^{m610} phenotype.

Taken together, these results suggest that specified neural crest cells accumulate at the level of the ventral neural tube border and do not enter the typical paths of migration to the pharyngeal arch regions. This could be due to an intrinsic inability of the cells to migrate because the normal developmental program was not activated, or due to an inadequate number of cells caused by a proliferation defect. To discriminate between these two possibilities, we tested the expression of genes critical for cell cycle progression and neural crest proliferation (*cyclin D1* and *id2*) but we have not been able to detect any changes in *mob*^{m610} at the level of

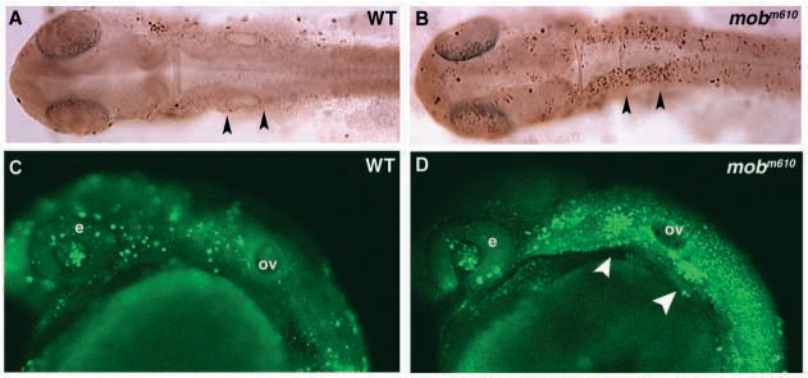

Fig. 9. Absence of *tfap2a* activity leads to increased levels of apoptosis in cranial neural crest. (A,B) Dorsal view of wild-type (A) and *mob*^{m610} (B) flat-mounted embryos at 26 hpf following TUNEL assay staining. Black arrowheads indicate the anterior and posterior extent of the otic vesicle. (C,D) Detection of dying cells by Acridine Orange staining of wild-type (C) and *mob*^{m610} mutant (D) embryos at 25 hpf (lateral views). White arrowheads indicate increased levels of apoptosis. ov, otic vesicle; e, eye.

mRNA expression (data not shown). In further experiments, we stained all proliferating cells in the larvae with an anti-phospho-histone 3 antibody (Link et al., 2001), but we did not detect any changes (data not shown). Thus, the mutation in *tfap2a* does not alter cell cycle progression, and allows normal proliferation rates of the neural crest cells.

Migrating *mob*^{m610} neural crest cells undergo apoptosis before they reach their final destination

Our results imply that cranial neural crest cells initially form in *mob* mutants but are unable to turn on their terminal differentiation program. Thus, these ill-fated neural crest cells might enter alternative pathways that lead to apoptosis, which may explain the lack of neural crest derivatives. To test this hypothesis, we have used the TUNEL assay and in vivo labeling with Acridine Orange to visualize apoptotic cells. In TUNEL assays we have detected increased chromatin fragmentation in dying cells at a time when neural crest cells disappear (Fig. 9A,B). In *mob*^{m610} mutants, we observed increased cell death in neural folds at 24 hpf that specifically affects the cranial crest of the second and posterior arches. We have independently confirmed these results in live embryos stained with Acridine Orange (Fig. 9C,D) where we observed a very specific accumulation of dying cells in the preotic and postotic streams of cranial neural crest at 24 hpf (Fig. 9D). These embryos were individually tracked and scored for the *mob* craniofacial phenotype at 3 dpf. These findings demonstrate that in the absence of *tfap2a* function, neural crest progenitors are specified and begin to migrate, but they are unable to maintain the differentiation process and undergo apoptosis.

Discussion

The TFAP2A transcription factor was first isolated from HeLa cells (Mitchell et al., 1987) and later found to regulate many genes active in a number of biological processes. In zebrafish and mouse, the gene is expressed in premigratory and later in early migratory neural crest cells. In addition, *Tcfap2a* is found in the branchial arch mesenchyme, cranial ganglia primordia, pericardial tissues, CNS, epidermis, limb mesenchyme and reno-urogenital tissues (Mitchell et al., 1991). Targeted disruption of the *Tcfap2a* gene revealed that the loss of function leads to a very dramatic phenotype of thoraco-abdominoschisis (Zhang et al., 1996; Schorle et al., 1996). Failure of body wall closure, severe malformations and deficits in the craniofacial skeleton made it difficult to identify a specific developmental role for *Tcfap2a.*

Tcfap2a belongs to a small family of nuclear proteins that bind as hetero- or homodimers to the palindromic core sequence 5′-GCCN$_3$GGC-3′ (Mohibullah et al., 1999). Other members include Tcfap2b (Moser et al., 1995), Tcfap2g (Bosher et al., 1996) and Tcfap2d (Zhao et al., 2001). Binding sites for these proteins were found in numerous developmentally regulated genes, e.g. *Erbb2* (Bosher et al., 1996), *KIT* (Huang et al., 1998) and *Hoxa2* (Maconochie et al., 1999). The TFAP2A protein contains a transactivation domain (P/Q rich region) and a basic and helix-span-helix region at the C terminus that constitutes the dimerization and DNA binding domains. Williams and Tjian (Williams and Tjian, 1991a; Williams and Tjian, 1991b) have shown that the C-terminal half of the protein is crucial for its function and that deletion of the last exon leads to loss of protein dimerization, DNA binding and transcriptional activity. Results of these DNA-binding studies were later exploited in designing DNA constructs for inactivation of the *Tcfap2a* gene by homologous recombination in the mouse (Zhang et al., 1996; Schorle et al., 1996).

We have cloned the zebrafish *mont blanc* locus and demonstrated that *mob*^{m610} mutation destroys the 3′ splice junction preceding the last exon (exon 7) of the zebrafish *tfap2a* gene. As a result, the splicing machinery is forced to use a cryptic splice site 14 bp into exon 7 that leads to a frame-shift and premature truncation of the protein. RT-PCR analysis specific for the deleted part of the gene did not reveal normally spliced message in the mutant embryos, which indicates that this mutation effectively abolishes the transcriptional activity of the Tfap2a protein. However, the question remains whether the variable phenotype of the *mob*^{m610} allele, as expressed by sporadic remnants of head cartilages, enteric neurons or DRGs, reflects residual Tfap2a activity due to an alternatively spliced allele, or whether some neural crest cells can develop normally in the complete absence of functional Tfap2a. To address this issue we have characterized the key phenotypes of the second zebrafish *mob*^{m819} allele that creates a premature stop codon deleting the last 2 exons (Holzschuh et al., 2003). We have carefully compared the phenotype of *mob*^{m610} and *mob*^{m819} mutant embryos and found that the craniofacial cartilage, neuronal (enteric, sympathetic, DRG, cranial ganglia) and all pigment cell phenotypes are identical between the two alleles (data not shown). Additionally, the apoptosis in the cranial neural crest streams showed the same severity in *mob*^{m819}

mutants (data not shown). Therefore, we conclude that the two mutations show the same level of *tfap2a* loss-of-function. The phenotype of the zebrafish mutations resembles the two mouse knockout lines where exon 5 (Schorle et al., 1996) and exon 6 (Zhang et al., 1996) were deleted. All four mutant lines obliterate transcriptional activity of the Tfap2a/Tcfap2a protein, and they can be considered as amorphic loss-of-function alleles. Because in zebrafish loss of Tfap2a activity does not affect either neurulation or body wall closure, we were able to study the specific function of Tfap2a in neural crest development.

tfap2a/*mob* is required for terminal differentiation of chondrogenic neural crest in pharyngeal arches 2 to 7, but not in the mandibular arch

The first pharyngeal arch forms normally in *mob* mutants and thus appears to be under a separate differentiation program that is not controlled by *tfap2a*. Crest of the first pharyngeal arch does not express Hox genes while the migratory cranial neural crest cells contributing to arches 2 to 7 are under the control of Hox genes, specifically *hoxa2*, *hoxb2* and *hoxa3* (Schilling et al., 2001). Expression of Hox genes (*hoxa2*, *hoxb2*, *hoxa3*) in *mob* mutant arches 2 to 7 is progressively diminishing, starting from 18 hpf when the facial primordia begin migration, and is almost completely absent by 24 hpf. In the mouse, *Hoxa2* confers second arch identity and its promoter contains a cranial neural crest enhancer built of three consecutive *Tcfap2a*-binding sites (Maconochie et al., 1999). This promoter structure is conserved in zebrafish where we also found multiple *tfap2a*-binding sites (A.B.-G. and E.W.K., unpublished). Similarly, it has been shown in zebrafish that the Hox paralogue group 2 (Hox PG2) specifies hyoid arch identity (Hunter and Prince, 2002). Results presented here are consistent with the hypothesis that in zebrafish *tfap2a* is acting upstream of Hox genes during the migration of the craniofacial primordia.

Furthermore, we have found that genes defining the chondrogenic neural crest, e.g. *wnt5a*, *sox9a* and *dlx2*, are greatly reduced in pharyngeal arches 2 to 7 in *tfap2a/mob*^{m610} mutant embryos, whereas they are normally expressed in the first arch. The expression of *wnt5a* commences in migrating chondrogenic crest around 18 hpf and persists in cartilage until beginning of chondroblast differentiation (~48 hpf), but it is absent in mature chondrocytes (Blader et al., 1996). Chondrocyte maturation defects were observed in all neural crest derived cartilages in the zebrafish mutation *pipetail/wnt5a* and also in *jellyfish/sox9a*, where final steps of cartilage terminal differentiation fail to proceed (Rauch et al., 1997; Piotrowski et al., 1996; Yan et al., 2002). Our data suggest that *wnt5a* and *sox9a* are regulated by *tfap2a* in Hox-positive pharyngeal arches but are under control of different regulatory pathways in the first pharyngeal arch.

Craniofacial cartilage patterns head paraxial mesoderm

Similar to other vertebrates, zebrafish head muscles are derived from paraxial mesoderm (Kimmel et al., 1990; Noden, 1983). The craniofacial cartilages and their corresponding muscles develop concurrently following the segmental pattern of pharyngeal arches (Schilling and Kimmel, 1997). Muscles originating from the paraxial mesoderm of the first and the second pharyngeal arch form the ventral set of muscles ima, imp (first arch), and ih, and hh (second arch; for abbreviations, see Results). In *mob*^{m610} mutant embryos we found that the orderly pattern of the striated cranial muscles was severely disrupted. Interestingly, lost or malformed muscles match the missing craniofacial cartilages on which the specific muscle inserts, but not the pharyngeal arch segment of paraxial mesoderm from which they originate. Specifically, the ventral muscle ima inserts on the Meckel's cartilage of first arch origin and it is always correctly formed and attached. By contrast, the imp muscles that connect Meckel's cartilage with ceratohyals (of second arch that are absent in *mob*^{m610} mutants) maintain correct rostral attachments to Meckel's cartilage. Caudally, however, the muscle fibers are loosely arranged and in some cases fused with ih or hh muscles that originate from the second arch. The ih and hh attach to hyoid arch cartilages and are present in most mutant embryos, although their morphology is distorted, preventing individual muscles from bundling correctly, and leaving scattered muscle fibers in the area anterior to the heart.

An interesting insight into muscle patterning comes from the analysis of dorsal muscles of the first two arches: do, lap, am (first arch) and ah, ao, lo (second arch). The am muscles, which originate from the first arch and connecting Meckel's cartilage with the palatoquadrate, which are both derived from the first pharyngeal arch, are always present in *mob*^{m610} mutants. However, the muscles lap and do, which are also of first arch origin but power skeletal elements of second pharyngeal arch origin, are consistently absent in *mob*^{m610} mutant embryos, as are the muscles ah, ao and lo, originating from the second arch segment and attaching to cartilages of second arch origin. Thus, it appears that the craniofacial mesenchymal condensations act as a source of inducing signals independently of the segmental origin of the paraxial mesoderm. Therefore, the lack of inducing centers for lap and do muscles leads to their loss but spares the am muscles. Alternatively (or additionally), *tfap2a* may cooperate with unknown factors that are necessary for specification of dorsal muscles but not ventral ones. These results reinforce the hypothesis originally put forward by Noden that neural crest derived chondrogenic condensations could be a source of patterning signals for paraxial mesoderm (Noden, 1983; Schilling and Kimmel, 1997).

Neural crest derivatives are depleted in *mob*^{m610}/*tfap2a* mutant embryos

The cranial ganglia receive contributions from ectodermal placodes and from neural crest as it was shown in avian systems (Le Douarin, 1982). In zebrafish detailed fate map studies of the cranial ganglia were not conducted, although it has been shown that the trigeminal ganglion contains cells of neural crest and placodal origin (Schilling and Kimmel, 1994). In *mob*^{m610} mutant embryos we found a reduction of cell numbers in the trigeminal (V), geniculate (VII) and nodose (X) ganglia, and a complete loss of the petrosal (IX) ganglion. The loss of cells in these ganglia is possibly due to requirement of *tfap2a* in the neurogenic placodes and/or contributing neural crest cells where the gene is expressed in mouse and in zebrafish. These results are in concordance with neurofilament immunohistochemistry findings in mouse knockout animals. Therefore, *tfap2a* may have similar

functions in cranial ganglia development in lower and higher vertebrates.

In *mob*^{m610}, trunk PNS neurons in the gut and the dorsal root ganglia are greatly reduced in numbers. Enteric neurons were not studied in the mouse knockout animals, but we would expect a similar phenotype to the zebrafish mutant. The zebrafish DRGs appear to be very sensitive to the depletion of functional *tfap2a*. The most striking and consistent phenotype is reduction of the number of cells per DRG to about half of its normal count. This might stem from an inadequate number of surviving progenitor cells to build individual ganglia and in some cases lack of ganglia when all cells have died. Interestingly, general inspection of mouse DRGs in the *Tcfap2a* knockouts did not show any deficits. It is possible that surviving zebrafish DRGs in *mob*^{m610} would eventually reach normal size by proliferation of existing progenitor cells. This cannot be ascertained in *mob*^{m610}/*tfap2a* mutants because they die before ganglia complete their development.

The function of *tfap2a* in melanocyte morphogenesis was not addressed in mice, because in the knockout animals the early phenotype of neural tube closure results in embryonic death before the onset of hair follicle development. In zebrafish, specification of pigment cells from neural crest precursors occurs before cells start to migrate, and by 18 hpf the first pigment lineage fated cells accumulate behind the eye (head melanoblasts) and behind the ear (trunk melanoblasts). An hour later, these cells begin expressing *dct* (*dopachrome tautomerase*) a gene that defines terminally differentiating melanoblasts and is also maintained in mature melanophores (cells equivalent to melanocytes in amniotes). During migration, the melanoblasts continue proliferating and are susceptible to patterning cues and trophic factors. We hypothesize that the reduced number and distribution of melanoblasts reflects a requirement for *mob/tfap2a* either for specification, migration, proliferation and/or survival. The fact that the number of differentiated melanophores and their dispersal improves with advanced development would argue that migration and proliferation do not depend on *mob/tfap2a* function and the initial loss of melanoblasts is due to either inadequate specification of progenitor cells or shortage of trophic factors required for survival. The first option can be excluded, because *mitfa* expression is only slightly delayed but maintained in pigment cell progenitors. Moreover, the tyrosine kinase receptor, *KIT*, has been shown to be a direct target of *TFAP2A* (Huang et al., 1998) and the zebrafish *kit/sparse* mutant exhibits a melanophore survival defect (Parichy et al., 1999). In *mob*^{m610} mutant embryos, *kit* expression is dramatically reduced but not completely absent. It is possible that other transcription factors maintain low levels of *kit* expression and allow later recovery of the melanophore pattern in *mob*^{m610} mutant embryos. Taken together, our data indicate that *mob/tfap2a* is required for regulation of target genes critical for survival of melanoblasts. Xanthophores appear to be similarly affected as the melanophores, but iridophores are more sensitive to loss of functional Tfap2a and they never recover.

tfap2a acts as a central regulator of terminal differentiation in migratory neural crest cells

We conclude that the early steps of neural crest induction and specification are not dependent on *tfap2a*, for the following reasons: first, genes defining neural crest progenitors (*foxd3*, *snail2*, *sox10*) are normally expressed at the 10-somite stage in the absence of *tfap2a*. Second, neural crest cells are able to migrate in the absence of *tfap2a*, as is clearly seen in the pigment cell lineages, first pharyngeal arch and the surviving cells of all other derivatives. A clear shift to dependence on *tfap2a* function in neural crest cell lineages is evident at 18 hpf. In the absence of *tfap2a*, migratory neural crest cells fail to express lineage specific genes (e.g. *dct*, *wnt5a*, *dbh*) and undergo apoptosis. Thus, *tfap2a* is required during a specific time window spanning the migratory neural crest and early phase of differentiation. We observed that progenitors of enteric neurons, DRGs and iridophores (etc.) initiate migration, but many of them die before reaching their destination and completing differentiation. In conclusion, it appears that all neural crest derivatives and placodes derived cranial ganglia depend on genetic pathways controlled by the *tfap2a* for survival and differentiation. Interestingly, some cells are able to escape the requirement for *tfap2a* and complete their development. One potential explanation for this phenomenon is that other transcription factors might be able to compensate for the loss of *tfap2a*. Similar to our results, different experimental approaches in mouse (Hilger-Eversheim et al., 2000), chick (Shen et al., 1997) and frog (Luo et al., 2003), found an increased apoptosis in neural crest cells and their derivatives in response to experimental or genetic depletion of Tfap2a.

Future analyses of the *mob* mutations will answer many remaining questions about gene hierarchy and gene-gene interactions governing morphogenesis of neural crest derivatives.

We thank Petra Hammerl and Christiane Knappmeyer for excellent technical assistance; Roland Nitschke for help with the confocal microscope experiments; Kristen Dutton and Robert Kelsh for sharing protocols and reagents; Elisabeth Kremmer for the anti-myosin antibody; and M. Ekker, M. A. Akimenko, V. Prince, M. Halpern, D. Parichy and B-C. Chung for providing plasmids for in situ hybridization. The authors appreciate helpful discussions and comments from the Driever, Knapik, Meyer and Varga laboratories. We are greatly indebted to Antonis K. Hatzopoulos and Iain Drummond for critical reading of the manuscript. This study was supported by: a Marie Curie fellowship from the 'Quality of Life' program (A.B.G.), the BMBF Grant AO-LS-99-MAP-LSS-003 (E.W.K.), and DFG Grants SFB 505 TP B7 and SFB 592 TP A3 (W.D.).

References

Akimenko, M. A., Ekker, M., Wegner, J., Lin, W., Westerfiled, M. (1994). Combinatorial expression of three zebrafish genes related to distal-less: part of a homeobox gene code for the head. *J. Neurosci.* **14**, 3475-3486.

Andermann, P., Ungos, J. and Raible, D. W. (2002). Neurogenin1 defines zebrafish cranial sensory ganglia precursors. *Dev. Biol.* **251**, 45-58.

Blader, P., Straehle, U. and Ingham, P. W. (1996). Three Wnt genes expressed in a wide variety of tissues during development of the zebrafish, Danio rerio: developmental end evolutionary prospectives. *Dev. Genes Evol.* **206**, 3-13.

Bosher, J. M., Totty, N. F., Hsuan, J. J., Williams, T. and Hurst, H. C. (1996). A family of AP-2 proteins regulates c-erbB-2 expression in mammary carcinoma. *Oncogene* **13**, 1701-1707.

Chiang, E. F. L., Pai, C. I., Wyatt, M., Yan, Y. L., Postlethwait, J. and Chung, B. C. (2001). Two Sox9 genes on duplicated zebrafish chromosomes: expression of similar transcription activators in distinct sites. *Dev. Biol.* **231**, 149-163.

Driever, W., Solnica-Krezel, L., Shier, A. F., Neuhauss, S. C. F., Malicki, J., Stemple, D. L., Stainier, D. Y. R., Zwartkruis, F., Abdelilah, S., Rangini, Z. et al. (1996). A genetic screen for mutations affecting embryogenesis in zebrafish. *Development* **123**, 37-46.

Dutton, K. A., Pauliny, A., Lopes, S. S., Elworthy, S., Carney, T. J., Rauch, J., Geisler, R., Haffter, P. and Kelsh, R. N. (2001). Zebrafish colourless encodes sox10 and specifies non-ectomesenchymal neural crest fates. *Development* **128**, 4113-4125.

Foernzler, D., Her, H., Knapik, E. W., Clark, M., Lerach, H., Postlethwait, J. H., Zon, L. I. and Beier, D. R. (1998). Gene mapping in zebrafish using Single-Strand Conformation Polymorphism analysis. *Genomics* **51**, 216-222.

Gans, C. and Northcutt, R. G. (1983). Neural crest and the origin of vertebrates: a new head. *Science* **220**, 268-274.

Goding, C. R. (2000). Mitf from neural crest to melanoma: signal transduction and transcription in the melanocyte lineage. *Genes Dev.* **14**, 1712-1728.

Hilger-Eversheim, K., Moser, M., Schorle, H. and Buettner, R. (2000). Regulatory roles of AP-2 transcription factors in vertebrate development, apoptosis and cell-cycle control. *Gene* **260**, 1-12.

Holzschuh, J., Barrallo-Gimeno, A., Ettl, A-K., Dürr, K., Knapik, E. W. and Driever, W. (2003). Noradrenergic neurons in the zebrafish hindbrain are induced by retinoic acid and require *tfap2a* for expression of the neurotransmitter phenotype. *Development* **130**, 5741-5754.

Huang, S., Jean, D., Luca, M., Tainsky, M. A. and Bar-Eli, M. (1998). Loss of AP-2 results in down-regulation of c-KIT and enhancement of melanoma tumorigenicety and metastasis. *EMBO J.* **17**, 4358-4369.

Hunter, M. P. and Prince, V. E. (2002). Zebrafish hox paralogue group 2 genes function redundantly as selector genes to pattern the second pharyngeal arch. *Dev. Biol.* **247**, 367-389.

Kelsh, R. N. and Eisen, J. S. (2000). The zebrafish *colourless* gene regulates development of non-ectomesenchymal neural crest derivatives. *Dev. Biol.* **225**, 277-293.

Kelsh, R. N. and Raible, D. W. (2002). Specification of zebrafish neural crest. *Results Probl. Cell Differ.* **40**, 216-236.

Kelsh, R. N., Dutton, K., Medlin, J. and Eisen, J. S. (2000a). Expression of zebrafish fkd6 in neural crest-derived glia. *Mech. Dev.* **93**, 161-164.

Kelsh, R. N., Schmid, B. and Eisen, J. S. (2000b). Genetic analysis of melanophore development in zebrafish embryos. *Development* **127**, 515-525.

Kimmel, C. B., Ballard, W. W., Kimmel, S. R., Ullmann, B. and Schilling, T. F. (1995). Stages of embryonic development of the zebrafish. *Dev. Dyn.* **203**, 253-310.

Kimmel, C. B., Warga, R. M. and Schilling, T. F. (1990). Origin and organization of the zebrafish fate map. *Development* **108**, 581-594.

Knapik, E. W., Goodman, A., Atkinson, O. S., Roberts, C. T., Shiozawa, M., Sim, C. S., Weksler-Zangen, S., Troillet, M. R., Futrell, C., Innes, B. A. et al. (1996). A reference cross DNA panel for zebrafish (Danio rerio) anchored with simple sequence length polymorphisms. *Development* **123**, 451-460.

Knapik, E. W., Goodman, A., Ekker, M., Chevrette, M., Delgado, J., Neuhauss, S., Shimoda, N., Driever, W., Fishman, M. C. and Jacob, H. J. (1998). A microsatellite genetic linkage map for zebrafish (*Danio rerio*). *Nat. Genet.* **18**, 338-343.

Knapik, E. W. (2000). ENU mutagenesis in zebrafish – from genes to complex diseases. *Mam. Genome* **11**, 511-519.

Knecht, A. K. and Bronner-Fraser, M. (2002). Induction of the neural crest: a multigene process. *Nat. Rev. Genet.* **3**, 453-461.

Le Douarin, N. M. (1982). *The Neural Crest*. Cambridge, UK: Cambridge University Press.

Link, B. A., Kainz, P. M., Ryou, T. and Dowling, J. E. (2001). The perplexed and confused mutations affect distinct stages during the transition from proliferating to post-mitotic cells within the zebrafish retina. *Dev. Biol.* **236**, 436-453.

Luo, T., Lee, Y. H., Saint-Jeannet, J. P. and Sargent, T. D. (2003). Induction of neural crest in Xenopus by transcription factor AP2alpha. *Proc. Natl. Acad. Sci. USA* **100**, 532-537.

Maconochie, M., Krishnamurthy, R., Nonchev, S., Meier, P., Manzanares, M., Mitchell, P. J. and Krumlauf, R. (1999). Regulation of Hoxa2 in cranial neural crest cells involves members of the AP-2 family. *Development* **126**, 1483-1494.

Manzanares, M. and Nieto, M. (2003). A celebration of the new head and a evaluation of the new mouth. *Neuron* **37**, 895-898.

Michelmore, R., Paran, I. and Kesseli, R. (1991). Identification of markers linked to disease-resistance genes by bulked segregant analysis: a rapid method to detect markers in specific genomic regions by using segregating populations. *Proc. Natl. Acad. Sci. USA* **88**, 9828-9832.

Mitchell, P. J., Wang, C. and Tjian, R. (1987). Positive and negative regulation of transcription in vitro: enhancer-binding protein AP-2 is inhibited by SV40 T antigen. *Cell* **50**, 847-861.

Mitchell, P. J., Timmons, P. M., Hébert, J. M., Rigby, P. W. J. and Tjian, R. (1991). Transcription factor AP-2 is expressed in neural crest cell lineages during mouse embryogenesis. *Genes Dev.* **5**, 105-119.

Mohibullah, N., Donner, A., Ippolito, J. A. and Williams, T. (1999). SELEX and missing phosphate contact analyses reveal flexibility within the AP-2 alpha protein: DNA binding complex. *Nucleic Acids Res.* **27**, 2760-2769.

Moser, M., Imhof, A., Pscherer, A., Bauer, R., Amselgruber, W., Sinowatz, F., Hofstadter, F., Schule, R. and Buettner, R. (1995). Cloning and characterization of a second AP-2 transcription factor: AP-2 beta. *Development* **121**, 2779-2788.

Neuhauss, S. C. F., Solnica-Krezel, L., Schier, A. F., Zwartkruis, F., Stemple, D. L., Malicki, J., Abdelilah, S., Stainier, D. Y. R. and Driever, W. (1996). Mutations affecting craniofacial development in zebrafish. *Development* **123**, 357-367.

Nieto, M. A. (2001). The early steps of neural crest development. *Mech. Dev.* **105**, 27-35.

Noden, D. M. (1983). The role of the neural crest in patterning of avian cranial skeletal, connective, and muscle tissues. *Dev. Biol.* **96**, 144-165.

Parichy, D. M., Rawls, J. F., Pratt, S. J., Whitfield, T. T. and Johnson, S. L. (1999). Zebrafish sparse correspondons to an orthologue of c-kit and is required for the morphogenesis of a subpopulation of melanocytes, but is not essential for hematopoiesis or primordial germ cell development. *Development* **126**, 3425-3436.

Parichy, D. M., Ransom, D. G., Paw, B., Zon, L. I. and Johnson, S. L. (2000). An orthologue of the kit-related gene fms is required for development of neural crest-derived xanthophores and a subpopulation of adult melanocytes in the zebrafish, Danio rerio. *Development* **127**, 3031-3044.

Piotrowski, T., Schilling, T. F., Brand, M., Jiang, Y. J., Heisenberg, C. P., Beuchle, D., Grandel, H., van Eeden, F. J. M., Furutani-Seiki, M., Granato, M. et al. (1996). Jaw and branchial arch mutants in zebrafish II: anterior arches and cartilague differentiation. *Development* **123**, 345-356.

Prince, V. E., Moens, C. B., Kimmel, C. B. and Ho, R. K. (1998). Zebrafish hox genes: expression in the hindbrain region of wild-type and mutants of the segmentation gene, valentino. *Development* **125**, 393-406.

Rauch, G. J., Hammerschmidt, M., Blader, P., Schauerte, H. E., Strähle, U., Ingham, P. W., McMahon, A. P. and Haffter, P. (1997). WNT5 is required for tail formation in the zebrafish embryo. *Cold Spring Harbor Symp. Quant. Biol.* **62**, 227-234.

Rawls, J. F., Mellgren, E. M. and Johnson, S. L. (2001). How the zebrafish gets its stripes. *Dev. Biol.* **240**, 301-314.

Richman, J. M. and Lee, S. H. (2003). About a face: signals and genes controlling jaw patterning and identity in vertebrates. *BioEssays* **25**, 554-568.

Rubinstein, A. L., Lee, D., Luo, R., Henion, P. D. and Halpern, M. E. (2000). Genes dependent on zebrafish cyclops function identified by AFLP differential gene expression screen. *Genesis* **26**, 86-97.

Schilling, T. F. and Kimmel, C. B. (1994). Segment and cell type lineage restrictions during pharyngeal arch development in the zebrafish embryo. *Development* **120**, 483-494.

Schilling, T. F. and Kimmel, C. B. (1997). Musculoskeletal patterning in the pharyngeal segments of the zebrafish embryo. *Development* **124**, 2945-2960.

Schilling, T. F., Prince, V. and Ingham, P. W. (2001). Plasticity in zebrafish hox expression in the hindbrain and cranial neural crest. *Dev. Biol.* **231**, 201-216.

Schorle, H., Meier, P., Buchert, M., Jaenisch, R. and Mitchell, P. J. (1996). Transcription factor AP-2 is essential for cranial closure and craniofacial development. *Nature* **381**, 235-238.

Shen, H., Wilke, T., Ashique, A. M., Narvey, M., Zerucha, T., Savino, E., Williams, T. and Richman, J. M. (1997). Chicken transcription factor AP-2: cloning, expression and its role in outgrowth of facial prominences and limb buds. *Dev. Biol.* **188**, 248-266.

Thisse, C., Thisse, B., Schilling, T. F. and Postlethwait, J. H. (1993). Structure of the zebrafish snail1 gene and its expression in wild-type, spadetail and no tail embryos. *Development* **119**, 1203-1215.

Thisse, C., Thisse, B. and Postlethwait, J. H. (1995). Expression of snail2, a second member of the zebrafish snail family, in cephalic mesoderm and

presumptive neural crest of wild-type and spadetail mutant embryos. *Dev. Biol*. **172**, 86-99.

Westerfield, M. (1995). *The Zebrafish Book*. Eugene, OR: University of Oregon Press.

Williams, T. and Tjian, R. (1991a). Analysis of the DNA-binding and activation properties of the human transcription factor AP-2. *Genes. Dev.* **5**, 670-682.

Williams, T. and Tjian, R. (1991b). Characterization of a dimerization motif in AP-2 and its function in heterologous DNA-binding proteins. *Science* **251**, 1067-1071.

Yan, Y.-L., Miller, C. T., Nissen, R., Singer, A., Liu, D., Kirn, A., Draper, B., Willoughby, J., Morcos, P. A., Amsterdam, A. et al. (2002). A zebrafish sox9 gene required for cartilage morphogenesis. *Development* **129**, 5065-5079.

Zhang, J., Hagopian-Donaldson, S., Serbedzija, G., Elsemore, J., Plehn-Dujowich, D., McMahon, A. P., Flavell, R. A. and Williams, T. (1996). Neural tube, skeletal and body wall defects in mice lacking transcription factor AP-2. *Nature* **381**, 238-241.

Zhao, F., Satoda, M., Licht, J. D., Hayashizaki, Y. and Gelb, B. D. (2001). Cloning and characterization of a novel mouse AP-2 transcription factor, AP-2delta, with unique DNA binding and transactivation properties. *J. Biol. Chem.* **276**, 40755-40760.